THE JOURNAL OF PHYSICAL CHEMISTRY A

 VOLUME 107, NUMBER 31, AUGUST 7, 2003

ARTICLES

Photodissociation of Formaldehyde in Rare Gas (Xe, Kr, Ar, and Ne) Matrixes

Kari J. Vaskonen and Henrik M. Kunttu*

Department of Chemistry, P.O. Box 35, 40014 University of Jyväskylä, Finland

Received: April 3, 2003; In Final Form: May 22, 2003

Infrared (IR) spectroscopy and electron paramagnetic resonance (EPR) are combined to study photodissociation of formaldehyde at photolysis wavelengths 308, 248, and 193 nm in rare gas matrixes. The photodissociation cross sections derived from the IR data show strong dependence on the matrix host and photolysis wavelength. Dissociation efficiency in Xe is 1−2 orders of magnitude higher than that in other matrixes. The kinetics of formation of atomic hydrogen and the final H atom concentration in the fully photolyzed sample vary significantly in different matrixes. In the 248 nm photolysis, the final number of H atoms in Kr and Ar matrixes is only $^1/_{20}$ and $^1/_{40}$ of the Xe matrix number, respectively. This behavior is discussed in the frame of a simple kinetic model. The anomalously fast dissociation at 193 nm in Xe matrix is discussed.

Introduction

Because of its structural and electronic properties, formaldehyde (H_2CO, FA) serves as an ideal prototype for a vast variety of photochemical and photophysical processes. Thus, electronic structure, spectroscopy, and photodissociation dynamics of FA has attracted a great deal of interest during the past decades, and FA is currently among the best-understood polyatomic molecules.[1−7] Besides purely academic interest, FA is an essential component of tropospheric photochemistry.[8] The first $\tilde{A}^1A_2(n,\pi^*) \leftarrow \tilde{X}^1A_1$ absorption of FA extends in the gas phase between 350 and 230 nm. This transition terminates on a bound electronic surface as indicated by the vibronic structure in the spectrum. Excitation within this manifold yields efficient vibronic coupling between the S_1 and S_0 surfaces and, consequently, population of highly excited vibrational levels of the ground state. In effect, this process leads to dissociation to molecular and radical products according to the scheme

$$H_2CO\ (S_0) + h\nu \rightarrow H_2CO\ (S_1) \rightarrow CO + H_2 \quad (1)$$

$$\rightarrow HCO + H \quad (2)$$

The radical channel (eq 2) has a threshold 0.3 eV higher than the molecular channel and possesses no energy barrier.[9] The state-to-state fragmentation dynamics and product state distributions of these processes are well characterized in the gas phase.[1−7] The next strong absorption of FA has an onset near 175 nm and is assigned to the Rydberg ($^1B_1(3s,n) \leftarrow \tilde{X}^1A_1$) transition.[10]

Photodissociation of several diatomic and triatomic molecules has been studied in rare gas crystals and matrixes.[11] Common to the previous studies is that dissociation is initiated by excitation within a strictly repulsive surface of the system. The excess energy above the bond dissociation energy is then partitioned among the fragments, and in a successful case, the lighter fragment overcomes the energy barrier and exits the parent cage permanently. FA clearly provides a nearly ideal system for studies on condensed phase effects on more complex photochemistry. In the present study, we have combined infrared spectroscopy (IR) and electron paramagnetic resonance (EPR) to investigate photodissociation of FA in rare gas (Rg) matrixes. It will be shown that photochemistry of FA is, as expected, complex and the matrix host influences strongly the efficiency of both photodissociation and production of atomic hydrogen. The experimental observations are discussed in the frame of a simple kinetic model. Condensed-phase photochemistry of FA

* To whom correspondence should be addressed. E-mail: Henrik.Kunttu@jyu.fi.

10.1021/jp0348676 CCC: $25.00
Published on Web 07/11/2003

monomer has been previously studied by Thomas and Guillory.[12] The main conclusion of this study was that the photochemistry of FA in Ar matrix is dominated by channel 1 yielding molecular dissociation products. It should be noted that this conclusion was based on observations by IR, which is blind for H atoms and not particularly sensitive for HCO.

Experimental Section

The gas samples were prepared in a 1 dm^3 Pyrex bulb connected to an all-glass vacuum manifold evacuated to 3×10^{-7} mbar with a diffusion pump. Two capacitance manometers (MKS Instruments) were used to obtain accurate guest-to-host ratios. The premixed gas mixture was deposited onto a cooled MgF_2 substrate with a typical flow rate of 0.02 mmol/min. The total amount of deposited gas was 2.3 mmol. Formaldehyde was released from paraformaldehyde (Sigma) according to the procedure by Spence and Wild.[13] Xe (99.997%, AGA), Kr (99.997%, AGA), Ar (99.999%, AGA), and Ne (99.997%, Messer Griesheim) were used at their nominal purities.

IR spectra were recorded with a Nicolet Magna IR 760 spectrometer equipped with a HgCdTe detector and a KBr beam splitter. A closed-cycle helium cryostat (APD Cryogenics, DE-202A) with a MgF_2 sample window and CaF_2 outer windows was used in the IR absorption measurements. The window cut off in this arrangement was at 1200 cm^{-1}. In some experiments, CsI widows were used. Ne matrixes were prepared in a liquid He transfer cryostat (Janis). EPR spectra were recorded with a Bruker ESP-300 series X-band spectrometer with 100 kHz magnetic field modulation. In the EPR measurements, the sample was deposited onto a flat copper target attached to the cryotip of a closed-cycle He cryostat (APD Cryogenics, DE-202S). Deposition temperatures of 25, 30, and 35 K were used to grow Ar, Kr, and Xe matrixes, respectively. Excimer lasers at 193 and 248 nm (Lambda Physik, Optex) and 308 nm (Estonian Academy of Sciences) were used to photolyze the samples.

Results

Infrared Observations. On the basis of the IR measurements, monomeric trapping of FA is obtained in Ar matrix when a 1:1000 FA/Ar gas sample is condensed at 20 K. The symmetric CH stretching vibration (ν_1) is located at 2798 cm^{-1}, and in more concentrated samples (1:100), the absorptions of FA dimer appear at 2803 and 2810 cm^{-1} and higher aggregates near 2819 cm^{-1}. Figure 1 illustrates this spectral region for matrixes with dilution ratios of 1:1000, 1:500, and 1:100. Kr matrixes deposited at 30 K and Ne matrixes deposited at 4.2 K yielded very similar observations as those in Ar. However, to obtain good dopant isolation combined with sufficient transparency of the matrix involves a compromise in choosing the deposition temperature. Thus, our Xe matrixes deposited at 35 K were somewhat snowy. The C−H stretching bands of FA monomer in different matrixes are shown in Figure 2.

Photolysis at the three laser wavelengths, 308, 248, and 193 nm, caused photodissociation of FA to some extent in all Rg matrixes. To quantify the efficiency of the photolysis, the integrated absorption intensity of the antisymmetric C−H stretching vibration near 2850 cm^{-1} was monitored as a function of the photolysis time. By extending the photolysis until a sufficient amount of FA was photobleached, a well-defined decay curve for kinetic analysis is obtained. Typical examples of such curves are presented in Figure 3. By assuming first-order decay kinetics, the curves can be fitted to a single exponential formula:

$$A(n) = A_0 \exp(-\gamma n) \qquad (3)$$

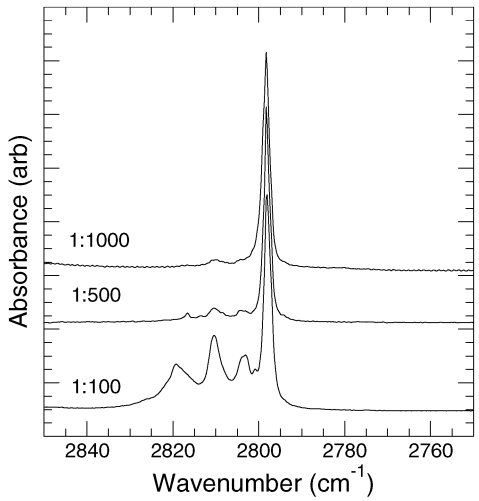

Figure 1. The symmetric C−H stretching vibration of FA in Ar matrix at different dilution. The spectral features on the high-energy side of the sharp monomer band are due to dimers and higher aggregates.

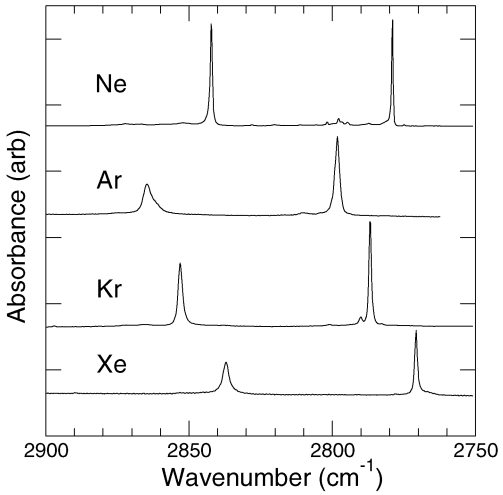

Figure 2. The antisymmetric (higher frequency) and symmetric (lower frequency) C−H stretching vibrations of FA in different matrix hosts.

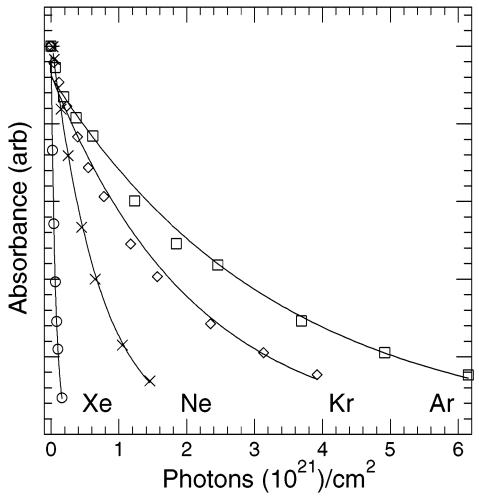

Figure 3. Decay of the IR absorption of FA in different matrixes. The photolysis wavelength is 248 nm. The data are fitted to first-order decay kinetics (eq 3).

TABLE 1: Cross Sections ($\gamma_1 + \gamma_2$, in 10^{-21} cm^2) of Formaldehyde Decay (IR) and Hydrogen Atom Production (γ', EPR) in Different Matrixes as Obtained from Single Exponential Fits (Eqs 3 and 4) of the Corresponding Data

wavelength (nm)	Xe	Kr	Ar	Ne
193	300 (IR)	2 (IR)	*b*	*c*
	600 (EPR)	4 (EPR)		
248	15 (IR)	1.3 (IR)	0.79 (IR)	1.4 (IR)
	4 (EPR)	1.9 (EPR)	1.7 (EPR)	
	20[a]	1[a]	0.5[a]	
308	1.5	0.09	*b*	*b*

[a] The (relative) final amount of atomic hydrogen in fully photolyzed samples. [b] No dissociation. [c] Not studied.

where A is the absorbance of the ν_1 band, n is the number of photons per square centimeter, and $\gamma = \gamma_1 + \gamma_2$ represents the total photodissociation cross section (in square centimeters) due to molecular and radical channels, respectively. The cross sections obtained in such way are collected in Table 1. Photodissociation of FA at 308 nm was very slow in all matrix hosts, and complete disappearance of the IR absorptions could not be achieved even with extensive irradiation. In Xe and Kr matrixes, the final extent of dissociation was 50% and 10%, respectively. Thus, the numerical values extracted for this wavelength suffer from some uncertainty. Noteworthy, no dissociation was observed in Ar matrix at 308 nm. Thermal annealing of the matrix has a strong effect on the photodissociation efficiency of FA in Xe matrix deposited at 30 K. Moreover, in samples not subject to annealing, the photolysis kinetics varied spatially in different parts of the matrix. Careful annealing of the matrix at 60 K yielded spatially uniform results and significant increase of the photolysis rate. Simultaneously, the decay curves turned to a single-exponential shape. The cross sections presented in Table 1 are obtained from annealed solids.

In more concentrated matrixes, photochemical processes due to FA dimers become important. A general observation in all matrix hosts was that dimers were very efficiently photobleached at all photolysis wavelengths. Parallel with the disappearance of the dimer, new bands appeared at 3541, 3549, and 3667 cm^{-1} when Ar matrix was photolyzed at 308 nm. On the basis of the analysis by Aspiala et al.,[14] these absorptions belong to the *Cc* and *Tg* conformers of glycolaldehyde. Quite interestingly, instead of glycolaldehyde, the main photochemical product of $(H_2CO)_2$ in Kr and Xe matrixes was the $CH_3OH{\cdot}CO$ complex.

The only stable photolysis product of monomeric FA that possesses IR activity is carbon monoxide. The CO absorption in 248 nm photolyzed Ar matrix appears as a single peak at 2138.0 cm^{-1}. Short annealing of the matrix at 30 K caused this absorption to split into three components with maxima at 2136.5, 2138.4, and 2139.7 cm^{-1}. These bands have been assigned to the CO−N_2 pair, the CO monomer, and the CO−CO pair, respectively.[15] In Kr matrix photolyzed at 248 nm the CO absorption showed maxima at 2136.3 and 2135.3 cm^{-1}. These peaks disappeared upon annealing, and a new absorption appeared at 2135.7 cm^{-1}. The 2135.7 cm^{-1} band has been assigned to the CO monomer.[15] Photolysis at 193 nm yielded CO absorption at 2135.6 cm^{-1} with a shoulder at 2136.8 cm^{-1}. In photolyzed Xe matrix the CO absorptions appeared at 2133.6 and 2133.1 cm^{-1}. Both peaks were resistant to annealing, and they most probably belong to the CO monomer. None of the CO absorption features can be unambiguously assigned to the CO−H_2 pair.

As manifested by formation of new hydrogen containing molecules, annealing of the photolyzed matrixes induces thermal mobility of trapped hydrogen atoms. IR spectra indicated formation of the HCO radical in all matrixes and xenon dihydride (HXeH) in Xe matrix.[16] The HCO radical is clearly a product of the thermally induced CO + H reaction. The relative amount of HCO can be estimated from the simultaneous decrease of the integrated CO absorption intensity. Results of such annealing experiments are collected in Table 2.

TABLE 2: The Effect of Annealing on the CO IR Absorption in Matrixes Fully Photolyzed at Different Wavelengths[a]

wavelength (nm)	Ar	Kr	Xe
248	0	1	20
193		40	20

[a] The numbers refer to the relative decrease in percentage.

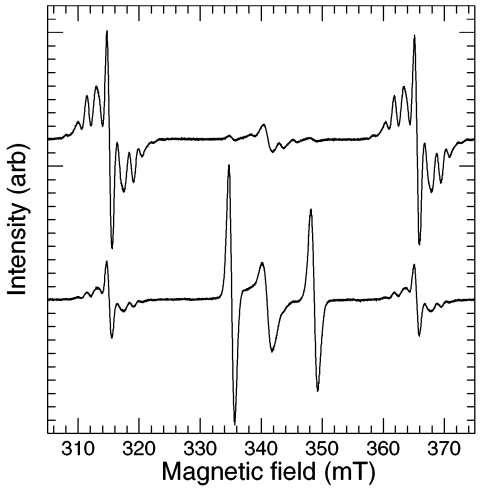

Figure 4. EPR spectra recorded from a photolyzed FA/Xe matrix: (top spectrum) directly after photolysis at 248 nm; (lower spectrum) after annealing the photolyzed matrix to 55 K. The structured doublet separated by 50.39 mT belongs to hydrogen atoms, whereas the doublet separated by 13.52 mT is due to the HCO radical.

Electron Paramagnetic Resonance. Two EPR spectra recorded from a photolyzed FA/Xe matrix are shown in Figure 4. The two main resonances seen possess isotropic hyperfine coupling constants of 50.39 and 13.52 mT and can be confidently assigned to hydrogen atom and formyl radical, respectively.[17,18] The pronounced substructure of the 50.39 mT doublet is caused by superhyperfine coupling of the electron spin of hydrogen atom to the nuclear spins of the neighboring magnetic ^{129}Xe and ^{131}Xe nuclei. Upon prolonged photolysis the hydrogen atom resonance gained intensity, whereas the formyl radical signal diminished and finally disappeared completely. This behavior is illustrated in Figure 5. In addition to these resonances, a broad unidentified feature is seen at 340 mT. Annealing of the photolyzed sample caused decrease of the hydrogen atom signal and simultaneous increase in the formyl radical and 340 mT signals. Very similar observations were made in FA/Kr matrix, whereas in Ar matrix, hydrogen atom was the sole direct paramagnetic photoproduct, and formyl radical appeared only after annealing of the matrix. The cryostat used in the EPR measurements does not provide sufficiently low temperature needed for Ne.

As shown in our previous report,[19] the strong isotropic EPR signal of the hydrogen atom provides a versatile probe for photodissociation of hydrogen-containing molecules. Moreover, the hyperfine coupling constant is sensitive to the matrix environment and, consequently, allows detailed analysis of trapping site structures.[20] The kinetics of hydrogen atom

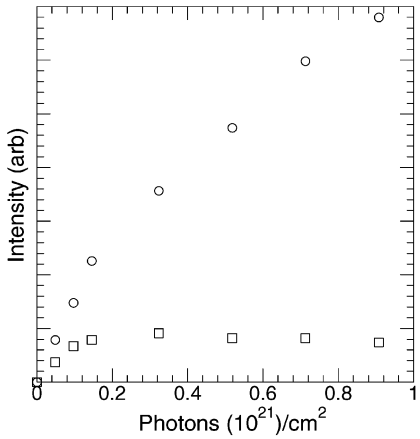

Figure 5. The behavior of the hydrogen atom (○) and the HCO radical (□) EPR signal intensities during 308 nm photolysis of a FA/Xe matrix.

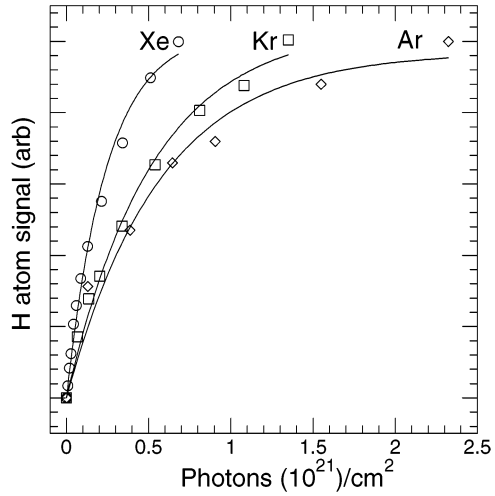

Figure 6. The relative hydrogen atom content in different matrix hosts as a function of the extent of photolysis at 248 nm. The lines represent single-exponential fits according to eq 4. The experimental signals are normalized to the same final value.

formation in the photolysis was followed in a similar manner as the decay of formaldehyde. The sample was irradiated by a known number of laser pulses after which the sample was placed inside the microwave cavity of the EPR spectrometer. This procedure was repeated until sufficient number of data points was obtained for reliable analysis. Care was taken to estimate the number of photons entering the sample during each laser pulse. Examples of growth curves of hydrogen atom density are presented in Figure 6. As will be discussed later, the kinetic scheme for hydrogen atom production from FA is rather complex, and several processes need to be considered. However, to provide a relative measure for production efficiencies in different matrix hosts and, moreover, to afford simple comparison with the IR decay curves, we at this point fit the data to a simple first-order kinetic formula,

$$S(n) = S_\infty[1 - \exp(-\gamma' n)] \qquad (4)$$

where S is the double-integrated EPR signal intensity and S_∞ its asymptotic value at infinite photolysis time. The cross sections γ' are collected in Table 1.

The double-integrated EPR signal is proportional to the absolute hydrogen atom density in the sample and thus provides a measure of hydrogen atom production. By careful sample preparation, it is, in principle, possible to estimate relative yields for different matrix hosts. These numbers, which clearly suffer from some experimental uncertainty, cannot be directly converted into branching ratio of the dissociation reaction; however, they provide useful information concerning the mechanism. Analysis of the EPR signals obtained from extensively irradiated solids show that the number of hydrogen atoms produced from constant amount of formaldehyde differs dramatically: the final value in Xe matrix was 20 times higher than that in Kr matrix and 40 times higher than that in Ar matrix (Table 1). The analysis of the site structure showed that the produced hydrogen atoms are mostly trapped in octahedral interstitial sites in Xe and Kr matrixes, whereas in Ar matrix a significant fraction of hydrogen atoms occupied substitutional sites. It should be noted, however, that the temperature of the EPR experiment was near the onset of diffusion of octahedrally trapped hydrogen atoms in Ar matrix.[21]

Because the intensity of an EPR resonance solely depends on the unpaired spin density and does not involve a molecule-dependent transition dipole like the IR transitions do, it is possible to provide quantitative estimates of the importance of different reaction channels responsible for the fate of thermally mobilized hydrogen atoms. The analysis of spectral changes during annealing indicates that 38% and 12% of the trapped hydrogen atoms reacted with carbon monoxide and produced HCO in Kr and Xe matrixes, respectively. A small amount, ca. 15%, of hydrogen atoms remained trapped after annealing. A further short photolysis period caused complete disappearance of the HCO radical and simultaneous recovery of the hydrogen atom population to 50% of its initial value. This would mean that at least 10% of the hydrogen atoms are released from traps other than HCO. Formation and dissociation of xenon dihydride[16] is consistent with this observation.

Discussion

As stated, the initial near-UV excitation of FA within the individual vibronic levels of the S_1 manifold promotes dissociation via two distinct channels in the gas phase. These channels lead to radical and molecular products with wavelength-dependent quantum yields ϕ_1 and ϕ_2, respectively. In addition, a few percent of the excited-state population relaxes by radiating. In the gas phase, emission is exclusively $S_1 \rightarrow S_0$ fluorescence,[22] but in heavier rare gases, also phosphorescence is observed.[23] In a solid matrix process, channel 2 means cage exit of the atomic product and subsequent stabilization of the separated pair. Photon absorption by the formed HCO radical then leads to formation of a more or less isolated CO molecule. The C−H bond enthalpy of HCO is only 0.7 eV.[9] If, on the other hand, internal molecular dissociation (eq 1) is effective, the hot fragments are born in the initial site of the parent molecule. Sufficient cooling provided by the neighboring lattice would then stabilize the CO−H_2 pair. The same final product could be formed by another mechanism peculiar to condensed-phase photochemistry. Here the CO−H_2 pair is an outcome of the in-cage hydrogen abstraction reaction H + HCO. The cage effect for hydrogen exit would enhance the probability of this reaction by extending the time that the reactive H atom spends in the initial site with HCO. In the gas phase, the H + HCO → H_2 + CO reaction has zero or slightly negative activation energy.[24] Unfortunately, the analysis of the present IR spectra does not provide a clear-cut answer whether CO−H_2 is formed in the photolysis. In conclusion, photochemistry of formaldehyde is complex in low-temperature matrixes, and the present data afford only some relatively general remarks.

The various reactions important for the FA photochemistry in matrixes can be simplified as

$$H_2CO + h\nu \xrightarrow{\gamma_1} H_2 + CO \quad (5)$$

$$H_2CO + h\nu \xrightarrow{\gamma_2} HCO + H \quad (6)$$

$$HCO + h\nu \xrightarrow{\gamma_3} H + CO \quad (7)$$

$$HCO + H + h\nu \xrightarrow{\gamma_4} H_2 + CO \quad (8)$$

The cross sections γ_1 and γ_2 define the total consumption of FA, which is monitored in the IR absorption measurements. Consequently, the single-exponential fits of the IR decay curves yield $\gamma_1 + \gamma_2$. It should be emphasized that, besides true molecular dissociation via channel 5, γ_1 includes molecular hydrogen production by the in-cage H + HCO → H_2 + CO mechanism. Reaction 6 corresponds to generation of a separated HCO···H pair in the lattice. Reaction 7 represents secondary photolysis of the HCO radical, and reaction 8 represents molecular hydrogen production in the photolysis of the HCO···H pair being formed in reaction 6. By limiting reaction 8 to closely separated pairs only, this reaction obeys first-order kinetics. We can now proceed and write the rate equations:

$$\frac{d[H]}{dn} = \gamma_2[H_2CO]_0\, e^{-(\gamma_1+\gamma_2)n} + \gamma_3[HCO] - \gamma_4[HCO] \quad (9)$$

$$\frac{d[HCO]}{dn} = \gamma_2[H_2CO]_0\, e^{-(\gamma_1+\gamma_2)n} - (\gamma_3 + \gamma_4)[HCO] \quad (10)$$

$[H_2CO]_0$ corresponds to the initial concentration of FA, and n is the number of photons/cm^2 delivered by the photolyzing laser. Equation 10 yields

$$[HCO] = \frac{[H_2CO]_0\gamma_2}{\gamma_3 + \gamma_4 - (\gamma_1 + \gamma_2)}\{e^{-(\gamma_1+\gamma_2)n} - e^{-(\gamma_3+\gamma_4)n}\} \quad (11)$$

The hydrogen atom concentration during the photolysis can be obtained by substituting eq 11 in eq 9 and integrating:

$$[H] = \phi_2[H_2CO]_0\left(1 + \frac{\gamma_3}{\gamma_3 + \gamma_4 - (\gamma_1 + \gamma_2)} - \frac{\gamma_4}{\gamma_3 + \gamma_4 - (\gamma_1 + \gamma_2)}\right)(1 - e^{-(\gamma_1+\gamma_2)n}) + (1 - 2\phi_3)[H_2CO]_0\left(\frac{\gamma_2}{\gamma_3 + \gamma_4 - (\gamma_1 + \gamma_2)}\right)(1 - e^{-(\gamma_3+\gamma_4)n}) \quad (12)$$

where $\phi_2 = \gamma_2/(\gamma_1 + \gamma_2)$ and $\phi_3 = \gamma_3/(\gamma_3 + \gamma_4)$ are the two branching ratios appearing in the proposed kinetic scheme.

Because the initial optical absorption of FA is the rate-determining step for hydrogen atom production, that is, $\gamma_3 + \gamma_4 \gg \gamma_1 + \gamma_2$, eq 12 simplifies to

$$[H] = 2\phi_2\phi_3[H_2CO]_0(1 - e^{-(\gamma_1+\gamma_2)n}) + (1 - 2\phi_3)\left(\frac{\gamma_2}{\gamma_3 + \gamma_4}\right)[H_2CO]_0(1 - e^{-(\gamma_3+\gamma_4)n}) \quad (13)$$

The relatively complex formula describing the time evolution of the hydrogen atom concentration contains several parameters, which obviously cannot be extracted from the present data. Nevertheless, we can inspect the effect of various parameters on the H atom production rate and final concentration. This could provide qualitative explanation to the very different photolysis behavior observed in different matrix hosts. For this purpose, the photolysis data at 248 nm seem most reliable. At this wavelength, the final amount of H atoms in Kr and Ar matrixes was $^1/_{20}$ and $^1/_{40}$ of the corresponding value in Xe, respectively. Moreover, the production rates of H atoms as represented by the simple first-order (eq 4) cross sections, γ', exceed the decay rates of FA in Kr and Ar, whereas in Xe matrix the situation is the opposite. These remarkable differences can be caused by variation in the two branching rations ϕ_2 and ϕ_3 appearing in eq 13. It can be easily seen that ϕ_2 has an effect on the final H atom concentration alone, whereas ϕ_3 affects also the shape of the growth curve by regulating the loss channel (eq 8). We demonstrate this behavior in Figure 7 for $\phi_3 = 1$, 0.5, and 0.1 cases. The other parameters are fixed as $\phi_2 = 0.5$, $\gamma_1 + \gamma_2 = 15 \times 10^{-21}$ cm^2, $\gamma_3 + \gamma_4 = 15 \times 10^{-20}$ cm^2, $\gamma_2/(\gamma_3 + \gamma_4) = 0.1$. Besides $\gamma_1 + \gamma_2$, which corresponds to the experimental value in Kr, we are forced to rely on estimates for the parameters. Although this treatment is semiarbitrary, it clearly shows that activation of the loss channel (eq 8) yields, simultaneously with reduction in the final H atom concentration, higher rates for H atom production. We believe that variation of ϕ_3 explains the experimental observations in the 248 nm photolysis, and it could be caused by a difference in flight distances of H atoms born from FA. It is quite expected that in the lighter rare gases the average distance in the HCO···H pair is shorter than that in Xe and could favor formation of molecular hydrogen in the secondary photolysis of HCO. In fact, annealing experiments do support this assumption.

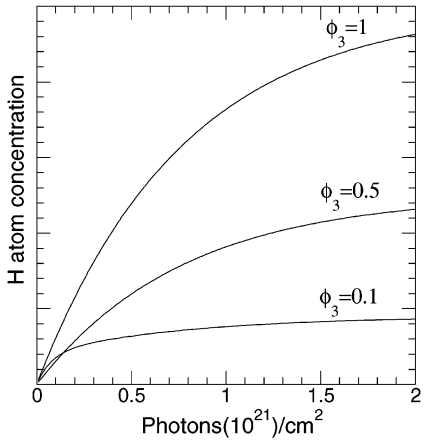

Figure 7. The effect of branching ratio ϕ_3 on the H atom production described by eq 13. The other parameters are fixed as $\phi_2 = 0.5$, $\gamma_1 + \gamma_2 = 15 \times 10^{-21}$ cm^2, and $\gamma_3 + \gamma_4 = 15 \times 10^{-21}$ cm^2.

Photodissociation of formaldehyde near 300 nm is very efficient in the gas phase. The total quantum yield, excluding fluorescence, is unity, and the molecular channel dominates by a factor of 4.[4] On the other hand, photolysis at 308 nm in low-temperature matrixes yields dissociation only in Kr and Xe. Moreover, the obtained dissociation cross sections, 1.5×10^{-21} cm^2 (Xe) and 0.09×10^{-21} cm^2 (Kr), are significantly smaller than the gas-phase value of 26×10^{-21} cm^2 for the FA absorption.[25] Because dissociation is initiated by absorption to discrete vibronic levels, conversion of these numbers to absolute quantum yields necessitates knowledge of the electronic absorption spectrum. Unfortunately, our attempts to record the $\tilde{A}^1A_2$-(n,π^*) ← $\tilde{X}^1A_1$ absorption in matrixes failed. Note that the energy of a 308 nm photon exceeds the thresholds of molecular

and radical channels by 0.6 and 0.25 eV, respectively.[6] The excess kinetic energy of hydrogen atom produced by the radical mechanism at 311 nm photolysis is only 0.16 eV.[9] For comparison, the barrier heights for hydrogen cage exit in H_2O/Rg matrixes typically exceed this number by more than 1 eV.[26] Thus, photodissociation of FA via the radical channel is surprising at this excitation energy and needs to be studied in more detail. The observation that FA dissociates significantly more slowly at 308 nm than at 248 nm, although 308 nm is near the gas-phase absorption maximum, might be ascribed to very low quantum yield of the molecular channel at this wavelength or to accidental mismatch between the photolysis wavelength and the absorption spectrum.

The 193 nm photolysis of FA shows anomalously large differences between Xe and other matrix hosts. The fact that FA does not dissociate in Ar at 193 nm is consistent with the known gas-phase profile of the $\tilde{A}^1A_2(n,\pi^*) \leftarrow \tilde{X}^1A_1$ transition, which does not extend below 230 nm.[25] In Kr matrix, both the dissociation efficiency and hydrogen atom production rate are, within obvious experimental errors, comparable to the 248 nm values. On the other hand, FA dissociates in Xe matrix very efficiently and production rate of hydrogen atoms exceeds the 248 nm photolysis by a factor of 150. It is clear that a difference of such magnitude cannot be ascribed to matrix effects. Moreover, a large blue shift of the $\tilde{A}^1A_2(n,\pi^*) \leftarrow \tilde{X}^1A_1$ system does not seem very likely. The experiments with different laser intensities exclude possible sequential two-photon processes as the origin for the surprising wavelength dependencies. Thus, we are left with an explanation that dissociation at 193 nm is caused by absorption of another electronic state, which is accessed in the heavier rare gases only. Our attempt to record absorption spectrum of FA in Xe matrix below 200 nm yielded a broad feature centered near 180 nm. Unfortunately, it is not clear whether this absorption belongs to FA. Finally, we note that the 193 nm photochemistry of hydrogen-donating species in Xe is strongly interfered by strong absorption (190 nm) and emission (250 nm) by the H/Xe exciplex.[27,28]

Conclusions

We have investigated photochemistry of FA in Rg matrixes and characterized photodissociation efficiencies together with production rates of atomic hydrogen at three excitation wavelengths. The motivation behind our effort is in extending our knowledge of condensed-phase effects on photodissociation of polyatomic molecules. It has been shown that the matrix environment has a crucial role in the observed photochemistry; moreover, dissociation and H atom production kinetics differ remarkably in different hosts. Because of the obvious complexity of the photochemistry, our main goal, that is, evaluation of the branching ratio between molecular and radical channels at different experimental conditions, was not unfortunately reached. To further quantify various photolytic processes, electronic absorption spectrum of matrix-isolated FA is needed. Furthermore, experiments with halogenated FA molecules, for example, HFCO, would definitely shed more light to the interesting condensed-phase photochemistry described in this investigation. Finally, we note that the role of the lowest triplet state in FA photochemistry needs to be considered in the future investigations.

Acknowledgment. The Academy of Finland supported this work.

References and Notes

(1) Moule, D. C.; Walsh, A. D. *Chem. Rev.* **1975**, *75*, 67.
(2) Houston, P. L.; Moore, C. B. *J. Chem. Phys*. **1976**, *65*, 757.
(3) Clark, J. H.; Moore, C. B.; Nogar, N. S. *J. Chem. Phys*. **1978**, *68*, 1264.
(4) Moortgat, G. K.; Warneck, P. *J. Chem. Phys*. **1979**, *70*, 3639.
(5) Butenhoff, T. J.; Carleton, K. L.; Moore, C. B. *J. Chem. Phys*. **1990**, *92*, 377.
(6) van Zee, R. D.; Foltz, M. F.; Moore, C. B. *J. Chem. Phys.* **1993**, *99*, 1664.
(7) Terentis, A. C.; Kable, S. H. *Chem. Phys. Lett*. **1996**, *258*, 626.
(8) Seinfeld, J. H.; Pandis, S. N. *Atmospheric Chemistry and Physics*; Wiley: New York, 1998.
(9) Chuang, M.-C.; Foltz, M. F.; Moore, C. B. *J. Chem. Phys*. **1987**, *87*, 3855.
(10) Brint, P.; Connerande, J.-P.; Mayhew, C.; Sommer, K. *J. Chem. Soc., Faraday Trans*. **1985**, *81*, 1643.
(11) Apkarian, V. A.; Schwentner, N. *Chem. Rev.* **1999**, *99*, 1481.
(12) Thomas, S. G.; Guillory, W. A. *J. Phys. Chem*. **1973**, *77*, 2469.
(13) Spence, R.; Wild, W. *J. Chem. Phys*. **1935**, 338.
(14) Aspiala, A.; Murto, J.; Sten, P. *Chem. Phys*. **1986**, *106*, 399.
(15) Dubost, H. *Chem. Phys*. **1976**, *12*, 139.
(16) Ahokas, J.; Kunttu, H.; Khriachtchev, L.; Pettersson, M.; Räsänen, M. *J. Phys. Chem. A* **2002**, *106*, 7743.
(17) Weltner, W., Jr. *Magnetic Atoms and Molecules*; Dover: New York, 1983.
(18) Adrian, F. J.; Cochran, E. L.; Bowers, V. A. *J. Chem. Phys*. **1962**, *36*, 1661.
(19) Eloranta, J.; Vaskonen, K.; Kunttu, H. *J. Chem. Phys*. **1999,** *110*, 7917.
(20) Kiljunen, T.; Eloranta, J.; Kunttu, H. *J. Chem. Phys*. **1999**, *110*, 11814.
(21) Vaskonen, K.; Eloranta, J.; Kiljunen, T.; Kunttu, H. *J. Chem. Phys*. **1999**, *110*, 2122.
(22) Miller, R. G.; Lee, E. K. C. *Chem. Phys. Lett*. **1975**, *33*, 104.
(23) Smith, J. J.; Meyer, B. *J. Chem. Phys*. **1969**, *50*, 456.
(24) Timonen, R. S.; Ratajczak, E.; Gutman, D. *J. Phys. Chem*. **1987**, *91*, 692.
(25) Rogers, J. *J. Phys. Chem*. **1990**, *94*, 4011.
(26) Schriever, R.; Chergui, M.; Schwentner, N. *J. Phys. Chem*. **1991**, *95*, 6124.
(27) Eloranta, J.; Kunttu, H. *J. Chem. Phys.* **2000**, *113*, 7446.
(28) Khriachtchev, L.; Pettersson, M.; Räsänen, M. *Chem. Phys. Lett.* **1998**, *288*, 727.